Pergamon

Journal of Structural Geology, Vol. 18, No. 1, pp. 27 to 39, 1996

0191-8141/96 $15.00 + 0.00

0191-8141(95)00085-2

Deformation mechanisms and inverted thermal profile in the North Almora Thrust mylonite zone, Kumaon Lesser Himalaya, India

PRAVEEN SRIVASTAVA and GAUTAM MITRA

Department of Earth and Environmental Sciences, University of Rochester, Rochester, NY 14627, U.S.A.

(*Received* 16 *April* 1992; *accepted in revised form* 19 *July* 1995)

Abstract—The thermal structure of a 2.2 km thick mylonite zone from the Kumaon Lesser Himalaya (India) is interpreted based on deformation mechanisms and microstructures. The mylonite zone lies along the North Almora Thrust (NAT), a S-dipping thrust that marks the northern flank of a large synformal crystalline klippe (Almora klippe), approximately 17 km north of the town of Almora. The mylonite zone evolved during the upper Eocene emplacement of the Almora klippe (part of a larger Munsiari thrust sheet), following the collision of India and Eurasia in lower–middle Eocene.

Mylonitic rocks near the top of the zone show dynamic recrystallization of both feldspar and quartz, indicating deformation at amphibolite grade (500–600°C). Near the center of the mylonite zone, the feldspars are fractured and quartz is dynamically recrystallized though to a lesser degree than near the top of the zone. This evidence, combined with the occurrence of secondary epidote + chlorite, biotite and calcite in these rocks, suggests that mylonitization occurred at greenschist grade (500–400°C). Near the base of the mylonite zone, biotite is present, feldspars are fractured and altered to sericite, and quartz shows limited plastic deformation in the form of undulose extinction and subgrain formation, indicating that temperatures of 400°C or less were reached during deformation. Deformation mechanisms and metamorphic reactions in the mylonite zone rocks thus point to a decrease in the temperature of deformation from 500–600°C near the top of the thrust zone to about 400°C near its base, suggesting an inverted thermal profile. We interpret this inverted thermal profile in the mylonite zone to have resulted from gradual cooling of the zone by heat transfer to a cold footwall at the time of thrusting.

INTRODUCTION

Descriptions of deformation mechanisms and microstructures of greenschist to amphibolite grade granitic mylonites are abundant in the literature. A wide variety of criteria are used for deducing the temperatures of mylonitization, thus establishing the link between temperature and deformation mechanisms operating in individual minerals. These criteria include: mineral assemblages in the mylonites and surrounding rocks (Mitra 1978, Debat *et al.* 1978, Vidal *et al.* 1980, Brown *et al.* 1980, Beach 1980, Hanmer 1982, Simpson 1985, Bell & Johnson 1989), oxygen isotope geochemistry (Kerrich *et al.* 1984, Kerrich & Hyndman 1986), feldspar geothermometry (LaTour & Barnett 1987), and experimental data (Tullis 1983, Tullis & Yund 1985). Deformation mechanisms and textures of feldspar and quartz are especially well known under greenschist to amphibolite grade conditions. In this study, we use deformation mechanisms and microstructures of feldspar and quartz as tools to deduce the temperatures of deformation and describe the thermal structure of a 2.2 km thick mylonite zone from the Kumaon Lesser Himalaya, India.

The mylonite zone lies in the hanging wall of the North Almora Thrust (NAT) which forms the northern S dipping margin of the synformal Almora klippe. The Almora klippe is the largest of a series of klippen that occur in the Lesser Himalaya of Kumaon. The NAT mylonite zone evolved during the emplacement of the Munsiari thrust sheet, the parent thrust sheet of the Almora klippe, in the upper Eocene, following the India–Eurasia collision in lower–middle Eocene (Molnar & Tapponier 1975, Powell 1979, Searle *et al.* 1987). The NAT zone is well exposed in a NE–SW transect near Takula, approximately 17 km north of Almora. We have mapped the mylonite zone in detail and have investigated mineralogical and grain size variations, shear sense indicators, and deformation mechanisms across the entire zone. We have also mapped the deformed sedimentary footwall of the NAT and examined deformation mechanisms.

Deformation mechanisms and microstructures of the hanging wall mylonites are described in this paper. Mylonitization temperatures are estimated from deformation mechanisms and metamorphic reactions. Evidence from these criteria suggests an inverted thermal profile in the NAT mylonite zone. Implications of this inverted thermal profile are discussed and a model leading to its development is suggested.

GEOLOGIC SETTING

In the Lesser Himalaya of Kumaon, several crystalline klippen tectonically overlie sedimentary rocks belonging to the Precambrian Damta and Deoban Groups and the Precambrian–Cambrian Jaunsar and Mussoorie Groups (Fig. 1; Valdiya 1980, Srivastava & Mitra 1994). At some places in the southern part of the area, the Paleocene–Eocene Subathu Formation (not shown in Fig. 1) lies unconformably over the Mussoorie Group and tectonically under the klippen, thus constraining the age of emplacement of the klippen (Munsiari thrust

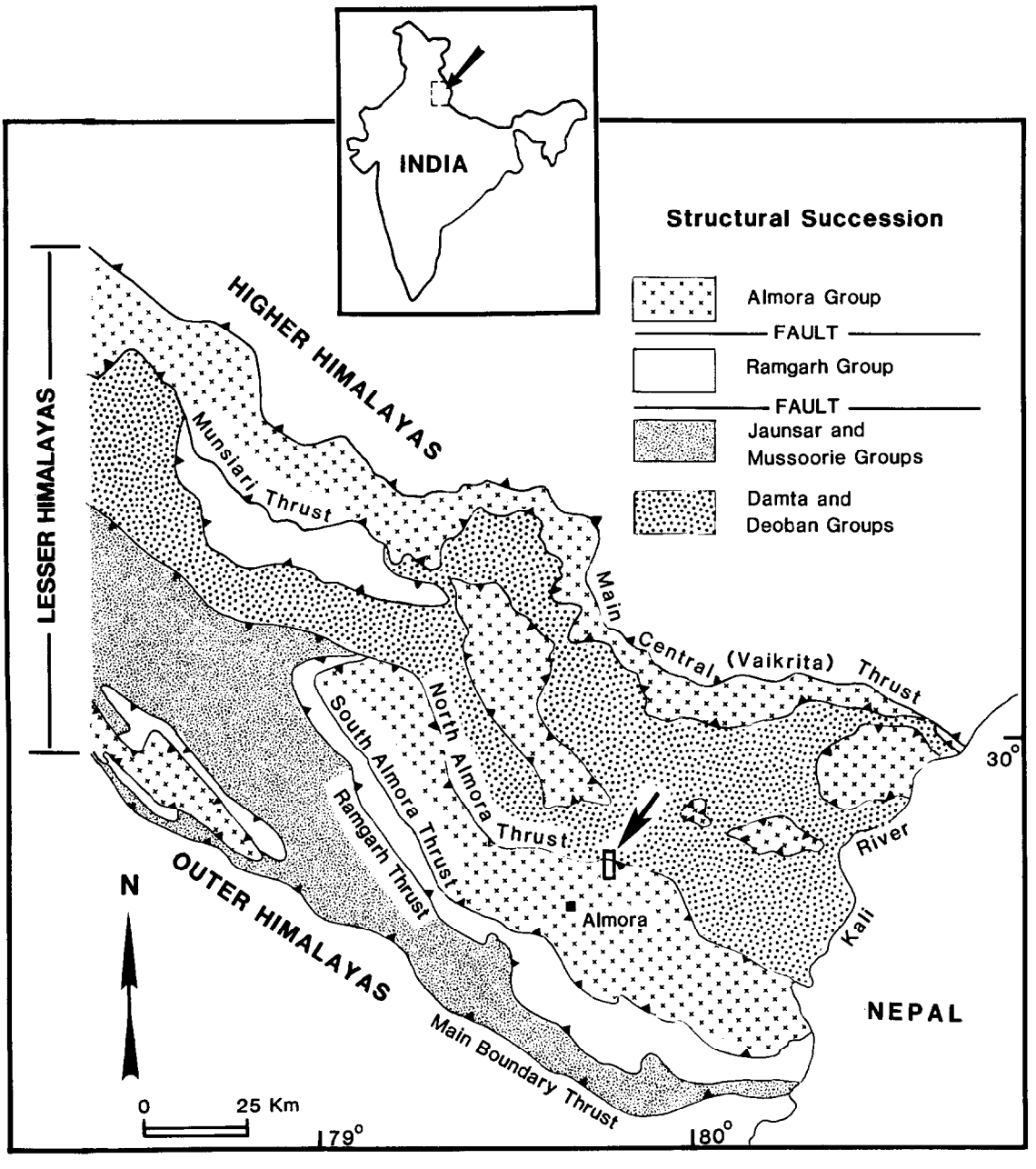

Fig. 1. Geologic map of the Kumaon Himalaya, India. Modified after Valdiya (1980).

sheet) as upper Eocene or younger (Srivastava 1992). The klippen consist of amphibolite grade metapelites, quartzites and augen gneisses belonging to the Precambrian Almora Group. At places, the greenschist grade metapelites of the Precambrian Ramgarh Group occur underneath the Almora Group, forming a series of lower klippen (Fig. 1).

The Almora klippe has apparently formed by erosion of a large synclinal fold in the crystalline Munsiari sheet, tectonically underlying the Main Central thrust sheet of the Higher Himalaya (Valdiya 1980, Srivastava & Mitra 1994). The NAT marks the northern boundary of the Almora klippe; its southern margin is bound by the South Almora thrust (SAT, Fig. 1). The klippe consists of a sequence of garnet–muscovite–biotite–quartz schist, muscovite–biotite–quartz schist, graphite–muscovite–quartz schist, quartzite and augen gneiss (Valdiya 1980). These mineral assemblages suggest an amphibolite grade metamorphism (Ghose *et al.* 1974). Preliminary geothermobarometric investigations of the metapelites have yielded temperatures of 475–575°C and pressures of 6–8 kb (Srivastava 1992). A number of granite bodies of regional extent intrude the metasedimentary rocks. One such granite body occurs near the town of Almora and has yielded a Rb/Sr whole rock crystallization age of 560 ± 20 Ma (Trivedi *et al.* 1984), suggesting that the metasedimentary rocks are at least Late Precambrian in age.

The study area is located approximately 17 km northeast of the town of Almora (Fig. 1). In this area, an excellent section of the NAT zone is exposed near the village of Takula, along the Almora–Bageshwar road

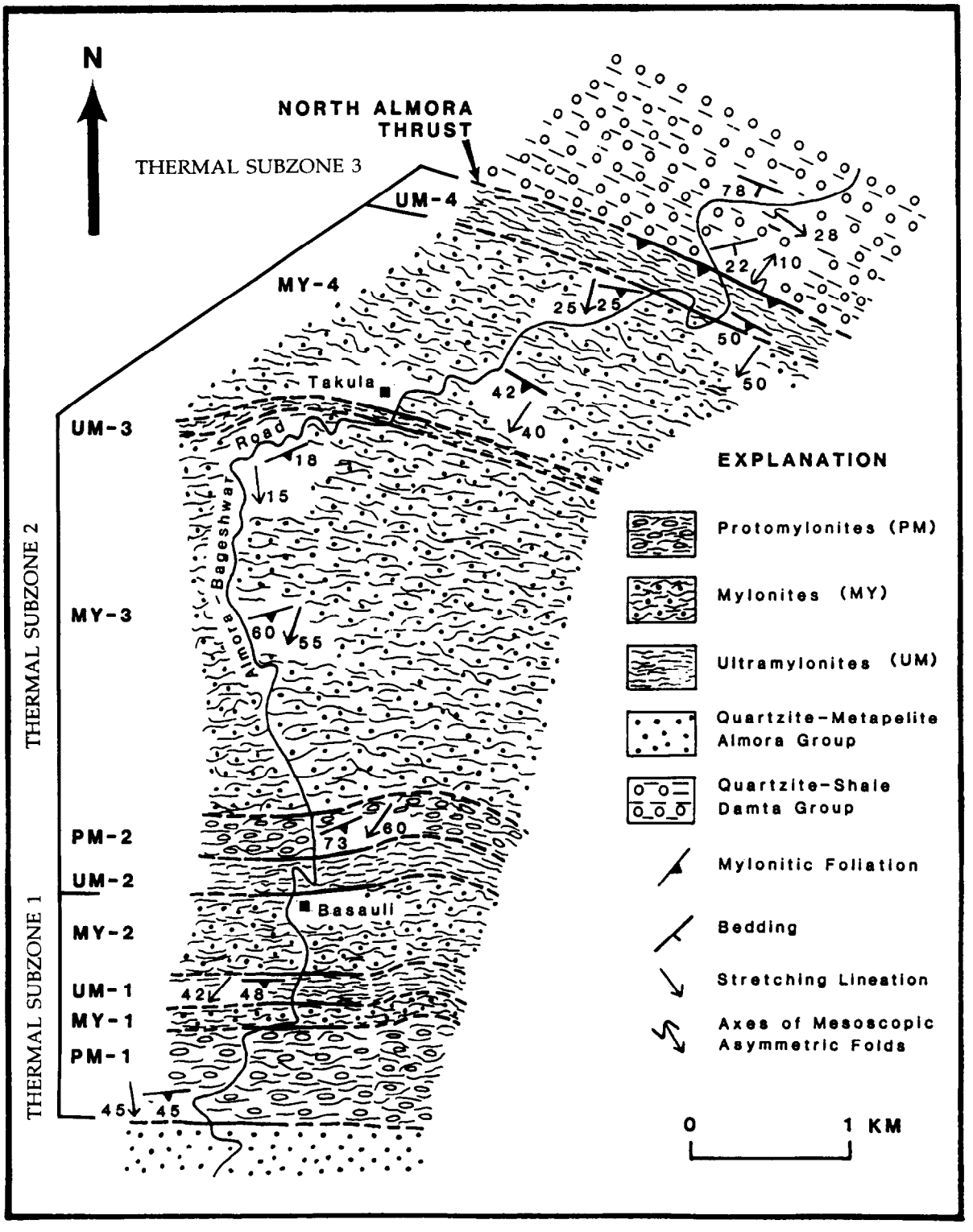

Fig. 2. Detailed geologic and structural map of the mylonite zone along the North Almora Thrust (NAT). The NAT is shown in the northern part of the map as the contact between the mylonitic rocks of the hanging wall and sedimentary units of the footwall. The thrust dips to the SW.

(Fig. 2). The NAT dips about 50° toward the southwest, with the hanging wall transported towards the southwest. The southwestward direction of transport along the entire NAT zone is shown by detailed outcrop and microscopic shear sense studies (Srivastava 1992). The thrust zone is defined in the Takula area by a 2.2 km thick mylonite zone that grades upward into the crystalline metamorphic rocks of the hanging wall (south of the fault), and overlies a 300 m thick zone of deformed sedimentary rocks of the footwall (north of the fault) (Fig. 2). The mylonites are granitic in composition and occur very consistently in the NAT zone along most of its strike length. Rb/Sr whole rock analysis of the mylonites has yielded dates in the range 1865 ± 60 Ma (Trivedi *et*

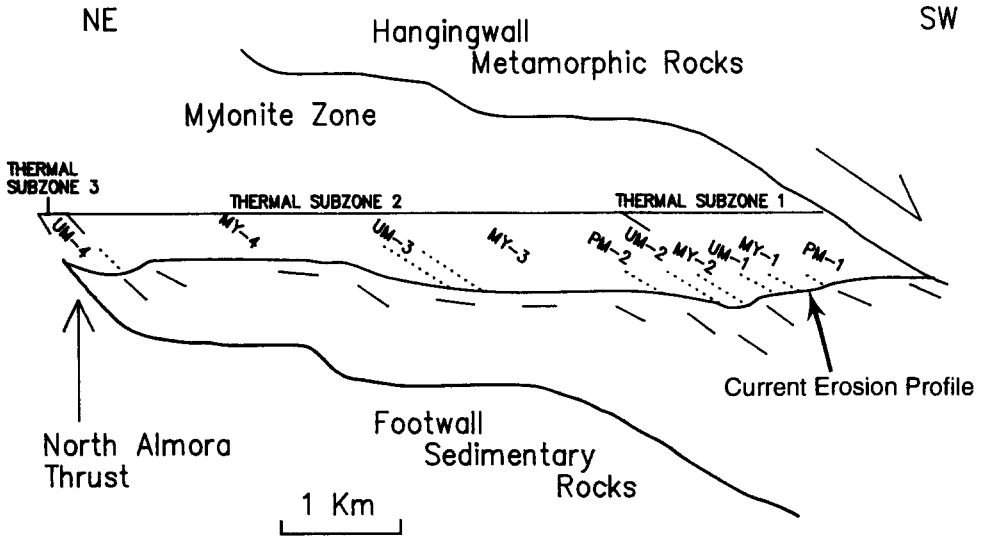

Fig. 3. The M-plane projection (M-pole = 0°, 146°) of the NAT mylonite zone. Dotted lines represent approximate locations of boundaries between protomylonite, mylonite, and ultramylonite zones shown in Fig. 2. The thin line across the mylonite zone reflects the approximate position of the current erosion profile.

al. 1984), probably reflecting the age of crystallization of the granitic protolith. Our field observations suggest that the mylonites originated from granites that were not intrusive into the hanging wall metasediments but rather represent the basement of the metasedimentary rocks. The footwall of the NAT in the study area consists of a quartzite–shale sequence of the Precambrian Damta Group (Fig. 2).

MYLONITE ZONE

The mylonites are a prominent feature of the NAT with a total outcrop width of about 6 km. A strong mylonitic foliation and a stretching lineation persist throughout the mylonite zone. The foliation dips toward the S or SW at 18–73° and the lineation plunges down the dip of the foliation at 15–60° (Fig. 2). An *M*-plane (Arthaud 1969, Angelier 1979, Aleksandrowski 1985, Marshak & Mitra 1988) projection of foliation orientation data shows that the mylonite zone is gently folded and is at least 2.2 km thick (Fig. 3). A detailed shear sense study across the mylonite zone has yielded a consistent top toward SW sense of shear (Srivastava 1992), suggesting that the entire zone probably developed during the episode of southward thrusting along the NAT.

Even though no undeformed protolith of the mylonitic rocks is present in the study area, mineral composition of some very coarse protomylonites, the least deformed rocks in the area, point to a granitic protolith. These protomylonites consists of quartz, K-feldspar, plagioclase, muscovite and biotite, with accessory zircon and apatite. Within the mylonite zone there are several alternating zones of protomylonites, mylonites and ultramylonites. Mineral assemblages found in each zone are listed in Table 1. For clarity of description, we have divided the mylonite zone into three thermal subzones that show evidence for successively lower temperatures of deformation towards the base of the mylonite zone (towards the north). Each of the thermal subzones is described below, beginning at the top (southern margin) of the mylonite zone. While interpreting the deformation mechanisms, we assumed that the average strain rate was approximately constant across the mylonite zone and that the effect of fluids on deformation mechanisms of minerals was mostly limited to areas close to the base (i.e. near the thrust) of the mylonite zone where the presence of fluids is indicated by abundant alteration

Table 1. Mineral assemblages encountered in the mylonite zone. Mineral symbols after Kretz (1983): Qtz—quartz, Bt—biotite, Kfs—K-feldspar, Pl—plagioclase, Ep—epidote, Chl—chlorite, Ca—calcite, Tur—tourmaline

Assemblage	Zones	Thermal subzones
Protomylonites		
1 Qtz + Ms + Bt + Kfs + Pl + Ep ± Chl	PM-1	1
2 Qtz + Ms + Bt + Kfs + Pl + Ep ± Chl	PM-2	2
Mylonites		
1 Qtz + Ms + Bt + Kfs + Pl	MY-1,2	1
2 Qtz + Ms + Bt + Kfs + Pl	MY-3,4	2
3 Qtz + Ms + Bt + Kfs + Pl + Ep	MY-3,4	2
4 Qtz + Ms + Bt + Kfs	MY-3	2
5 Qtz + Ms + Bt + Kfs + Pl + Ep + Chl	MY-3	2
6 Qtz + Ms + Bt + Kfs + Pl + Ca	MY-4	2
7 Qtz + Ms + Bt + Kfs + Ep + Chl	MY-4	2
Ultramylonites		
1 Qtz + Ms + Bt + Kfs + Pl + Chl	UM-1	1
2 Qtz + Ms ± Kfs ± Pl + Ep + Chl	UM-2	2
3 Qtz + Ms + Chl + Kfs	UM-3	2
6 Qtz + Ms ± Bt	UM-4	3
7 Qtz + Ms + Bt + Kfs ± Pl	UM-4	3
9 Qtz + Ms ± Bt ± Kfs + Tur	UM-4	3
10 Qtz + Ms + Bt + Chl + Tur	UM-4	3

of feldspars to white mica. Even if fluids infiltrated farther into the hanging wall (as indicated by some feldspar alteration away from the fault), this would only lower the absolute temperature estimates in each zone but not change the relative temperature of one thermal subzone with respect to another. In our interpretation of the microstructures, we have assumed temperature to be the main factor controlling the deformation mechanisms of minerals. This point is further elaborated below.

Thermal subzone 1

This subzone includes the protomylonites PM-1, mylonites MY-1 and MY-2, and ultramylonites UM-1 (Fig. 2).

Feldspar. Feldspar is plastically deformed throughout the subzone (Fig. 4a). In the protomylonites (PM-1), K-feldspar and plagioclase porphyroclasts smaller than 0.5–1.0 mm in diameter are plastically deformed but larger porphyroclasts (up to 5 mm diameter) are primarily fractured. A similar phenomenon was described by Mitra (1978) from Blue Ridge mylonites in the Appalachians and by Tullis & Yund (1985) from experimentally deformed K-feldspar. Some plastically deformed feldspar porphyroclasts have recrystallized grains (0.15–0.25 mm) at their boundaries, while others are completely recrystallized. Most recrystallized grains show either cross-hatched or polysynthetic albite twinning (similar to Fig. 4a). Some of the recrystallized grains exhibit strong undulose extinction, suggesting that they have been further deformed. Aggregates of recrystallized K-feldspar and plagioclase grains occur in the matrix along with recrystallized quartz.

In the mylonites (MY-1 and MY-2), feldspar grains in the size range 0.8–1.2 mm are plastically deformed, while larger feldspar grains are fractured. The plastically deformed porphyroclasts are dynamically recrystallized (into 0.1 mm grains), either completely or show a core–mantle structure (Fig. 4a; Debat *et al.* 1978, Vidal *et al.* 1980). Recrystallized K-feldspar grains have straight or curved boundaries and form equilibrium triple junctions (Fig. 4a). Plagioclase porphyroclasts ($\leq$ 0.6 mm) are typically smaller than K-feldspar porphyroclasts in the same sample, and show evidence of plastic deformation by way of deformation twins (White 1975).

In both the protomylonites and mylonites, feldspar porphyroclasts larger than ~1.0 mm have undergone two phases of fracturing. The first phase fractures (Fig. 4b) are similar to the high temperature albite filled fractures described by Debat *et al.* (1978). The second phase fractures are widely spaced (1–2 mm), may occur in single or conjugate sets, and are filled with equant recrystallized quartz grains (Fig. 4b).

The ultramylonites (UM-1) are relatively coarse grained compared to the ultramylonites of other thermal subzones (UM-2, 3 and 4). Feldspar porphyroclasts (~1 mm diameter) in these rocks show dynamic recrystallization, weak undulose extinction and minor fracturing.

Retrogressive alterations of K-feldspar and plagioclase to muscovite + quartz (sericitization) is common in all these rocks, evidently associated with the cooling of the mylonite zone.

Quartz. Quartz has undergone extensive dynamic recrystallization in the protomylonites (PM-1) and mylonites (MY-1 and MY-2) and no quartz porphyroclasts remain. In PM-1, quartz ribbons are up to 0.8 mm wide and lensoid in shape (Fig. 4c) with bulbous middle portions often consisting entirely of recrystallized grains. The bulbous portions represent original quartz porphyroclasts, as indicated by the local presence of unrecrystallized cores. In the mylonites (MY-1 and MY-2), quartz occurs as recrystallized grains (0.15 mm) in ribbons and in asymmetric tails of feldspar porphyroclasts. A few quartz porphyroclasts, up to 1.5 mm in diameter, do remain in the ultramylonites UM-1. Small porphyroclasts show little deformation, while large ones (~1 mm) display strong undulose extinction and recrystallization. Lensoid quartz ribbons consisting of recrystallized grains (~0.15 mm) are also common.

Phyllosilicates. Muscovite and biotite are newly crystallized in the protomylonites (PM-1) and mylonites (MY-1 and MY-2) (cf. Etheridge & Hobbs 1974, Wilson & Bell 1979) and define the mylonitic foliation. However, the two minerals are coarser in the protomylonites (average size: 0.25 × 0.10 mm) than in the mylonites (average size: 0.12 × 0.02 mm). In the ultramylonites (UM-1), biotite and muscovite are approximately 0.15 × 0.05 mm in size. A few biotite grains in PM-1 show retrogression to chlorite (Fig. 4d). There is substantial retrogression of biotite to chlorite in the UM-1 ultramylonites. Retrogression of biotite to chlorite is evident from the fact that chlorite is almost always either surrounded by or intergrown with biotite (Fig. 4d) and the boundaries between the two minerals are at times indistinct. Biotite grains in such cases are cloudy and show a gradation from the brown colour of biotite to the green colour of chlorite under plane polarized light. A few small chlorite grains occur in the matrix independent of biotite; these chlorite grains probably formed from complete retrogression of biotite into chlorite.

Plastic deformation of feldspar and quartz, and formation of biotite along the main mylonitic foliation, are considered syntectonic processes with respect to the main phase of deformation in the thermal subzone 1. Formation of chlorite in this thermal subzone appears to be a late phenomenon (post-tectonic) with respect to both the plastic deformation of feldspar and formation of biotite. Chlorite grains are, however, not seen to cross-cut the mylonitic foliation probably because chlorite grew in the same orientation as the parent biotite and at lower temperatures but under the same overall movement direction and strain field along the NAT.

Temperature of deformation. Dynamic recrystallization of K-feldspar is usually seen in amphibolite grade (500–600°C) mylonites (Debat *et al.* 1978, Vidal *et al.* 1980, Hanmer 1982, Tullis 1983 and references therein,

Bell & Johnson 1989). Under the same conditions, plagioclase deforms mainly by fracturing (Debat *et al.* 1978). White (1975), however, described limited recrystallization in oligoclase by nucleation mechanisms at lower amphibolite grade. Recrystallization by progressive subgrain rotation is found in intermediate plagioclases at upper amphibolite to granulite grade conditions (cf. Vernon 1975, Voll 1976, Brown *et al.* 1980, Hanmer 1982, Tullis 1983, Bell & Johnson 1989). Thus it appears that recrystallization in plagioclase takes place at a higher temperature than K-feldspar. We infer that the temperature of mylonitization in thermal subzone 1 must have been 500–600°C or higher near the southern margin of the NAT zone because both K-feldspar and plagioclase have recrystallized in this area. These are the highest temperatures of mylonitization encountered in the NAT mylonite zone. The presence of chlorite in PM-1 and UM-1 as a retrogressive mineral after biotite records the cooling history of thermal subzone 1 through lower temperatures. As discussed later, the cooling of the subzone may be a result of the transfer of heat to the footwall under an inverted thermal gradient.

Thermal subzone 2

This subzone consists of protomylonites PM-2, mylonites MY-3 and MY-4, and ultramylonites UM-2 and UM-3 (Fig. 2).

Feldspar. In PM-2 protomylonites, plagioclase porphyroclasts are smaller in size (2–3 mm diameter) and less abundant than K-feldspar porphyroclasts (5–6 mm diameter). A similar relation between the two feldspars is also seen in the mylonites (MY-3 and MY-4), though the overall size of plagioclase and K-feldspar is smaller, 1.0–1.25 mm and 2.0–3.0 mm diameter, respectively. The dominant mechanism of feldspar deformation in the protomylonites and mylonites is fracturing. However, a few feldspars show limited plastic deformation in the form of weak to strong undulose extinction (K-feldspar) or deformation twinning (plagioclase). Fractures in feldspars are either parallel to the cleavage planes or occur in conjugate sets independent of the cleavage; a large number of fractures are at high angle (70–90°) to the main foliation. In the mylonites (MY-3 and MY-4), fracturing of feldspars is more common in samples containing a large number of porphyroclasts and a coarse matrix (cf. Debat *et al.* 1978, Vidal *et al.* 1980). Although both feldspars show retrogressive alteration throughout the subzone, plagioclase has undergone more alteration than K-feldspar and has completely disappeared in some cases. Alteration is most pronounced in mylonites from the northern half of MY-4, where fracturing becomes a minor deformation process. Chemically, feldspar alteration involves sericitization of both the feldspars, and formation of epidote + muscovite or calcite + muscovite + biotite from the plagioclase.

Feldspar porphyroclasts are rare in the ultramylonites (UM-2 and UM-3). Where found, the feldspar porphyroclasts are 0.1–0.2 in diameter and are relatively undeformed, although some may show a weak undulose extinction. Sericitization of the feldspars is common in the ultramylonites.

Quartz. Quartz porphyroclasts in PM-2 protomylonites show strong undulose extinction and dynamic recrystallization (Fig. 5a). Recrystallized grains occur in irregular patches and along linear zones within large porphyroclasts (~5 mm diameter), and along their boundaries, especially where asymmetric tails join the porphyroclasts. Recrystallized grains are equiaxed (0.25–0.30 mm) with straight or slightly wavy boundaries and form equilibrium triple junctions (Fig. 5a).

Quartz porphyroclasts (0.45–2.0 mm diameter) are very common in the mylonites of MY-3 and southern half of MY-4. The porphyroclasts show strong undulose extinction, formation of crude deformation bands (Hobbs *et al.* 1976), and core–mantle structure (White 1976). Quartz porphyroclasts are less common in the northern half of MY-4 and show undulose extinction, subgrain formation, and dynamic recrystallization.

No quartz porphyroclasts occur in the ultramylonites of UM-2. Quartz occurs in lensoid 0.1–0.5 mm thick layers consisting of recrystallized grains (0.02–0.05 mm) and the quartz layers alternate with 0.2 mm thick layers of muscovite. In the ultramylonites of zone UM-3, quartz layers, ~1.0 mm thick and consisting of recrystallized porphyroclasts (up to 1 mm diameter) and recrystallized grains (0.05–0.1 mm), alternate with layers of muscovite and chlorite (see below). Rarely, isolated quartz porphyroclasts (0.1 mm) showing weak undulose extinction also occur.

Phyllosilicates. Muscovite and biotite are 0.25 × 0.10 mm (average) in size in the protomylonites (PM-2), whereas in the mylonites they are much finer (0.16 × 0.02–0.03 × 0.01 mm). Both the minerals are undeformed throughout subzone 2 and appear to be newly crystallized, except where biotite has partially altered to post-tectonic chlorite (northern part of MY-4). In the UM-2 ultramylonites, which consist of mostly muscovite and quartz, 0.2 mm thick layers of muscovite alternate with 0.1–0.5 mm thick layers of recrystallized quartz. Muscovite also defines a crenulation cleavage in UM-2, which is more pronounced than the older isoclinally folded foliation. The UM-3 ultramylonites consist of mostly muscovite and chlorite, and the several mm thick layers of the two minerals alternate with ~1.0 mm thick layers of quartz. Syntectonic chlorite is found throughout thermal subzone 2, occurring in porphyroclast tails (Fig. 5b), in the matrix, and within feldspar porphyroclasts. Post-tectonic chlorite occurs in the northern part of MY-4, having formed from retrogression of biotite, and in a few samples of UM-2 and UM-3, occurring in lensoid aggregates with fibers growing almost perpendicular to the main foliation.

Temperature of deformation. In the protomylonites (PM-2) and mylonites (MY-3 and MY-4), both K-

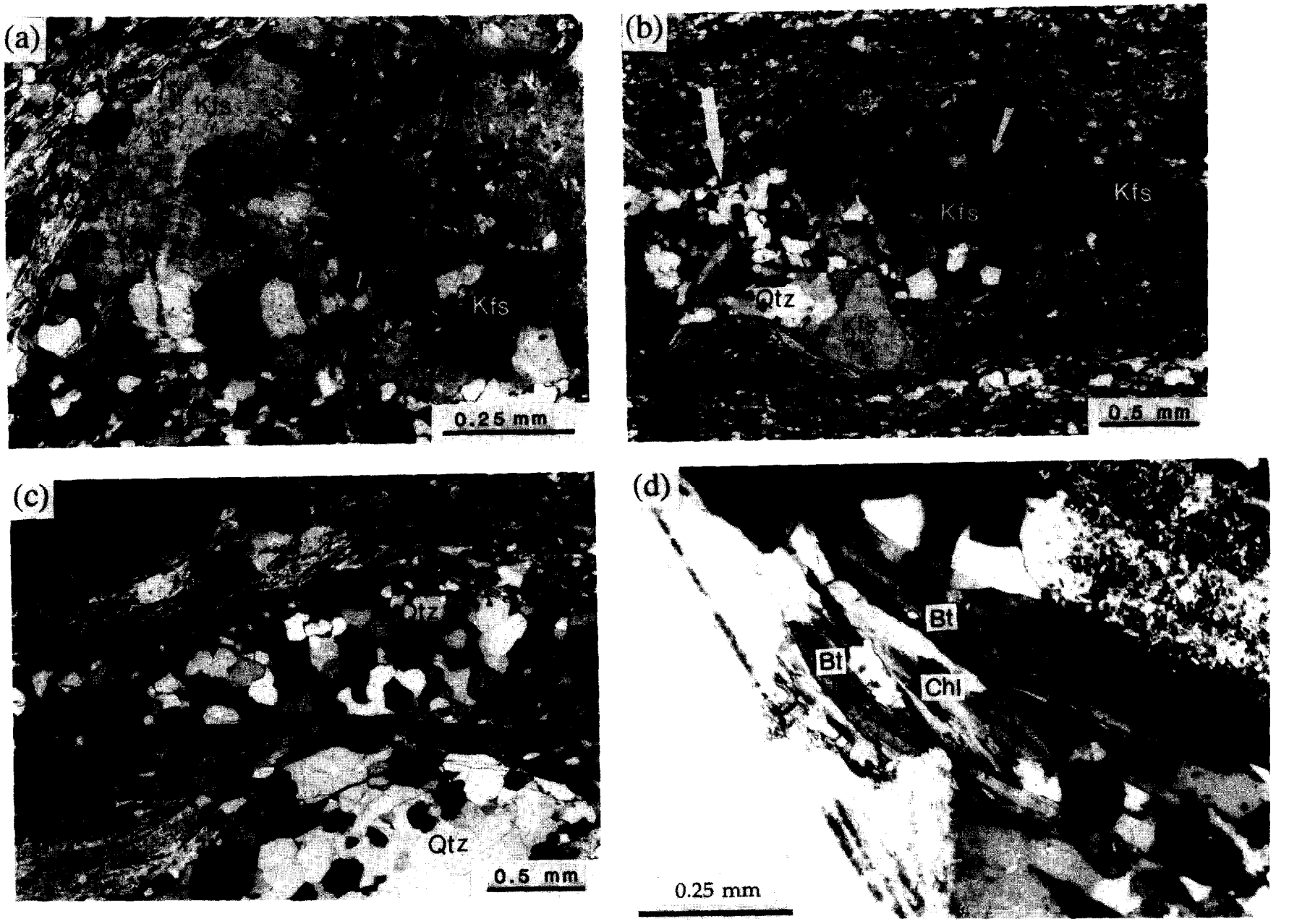

Fig. 4. (a) Recrystallized K-feldspar porphyroclast in a mylonite from thermal subzone 1. Most of the recrystallized grains are of similar size (~0.1 mm). The porphyroclast is surrounded by a matrix of quartz and muscovite in the upper and lower left-hand corners. (b) Fractures of two phases in a mylonite of thermal subzone 1. The first phase fractures (marked by the smaller arrow) appear as linear zones of lighter color (filled with albite) than the host grain. The second phase fractures are occupied by recrystallized quartz; one such fracture is shown in the left half of the picture (marked by the bigger arrow). (c) Complete dynamic recrystallization of quartz porphyroclasts into ribbons in a protomylonite of thermal subzone 1. Quartz ribbons have bulbous portions representing original quartz porphyroclasts. (d) Retrogressive chlorite among older biotite, under crossed-polars. Chlorite has an acicular habit and its boundaries and color under plane polarized light are gradational with biotite. Biotite and chlorite grains are cloudy near their mutual boundaries. Top is upward and north is to the left in all photomicrographs.

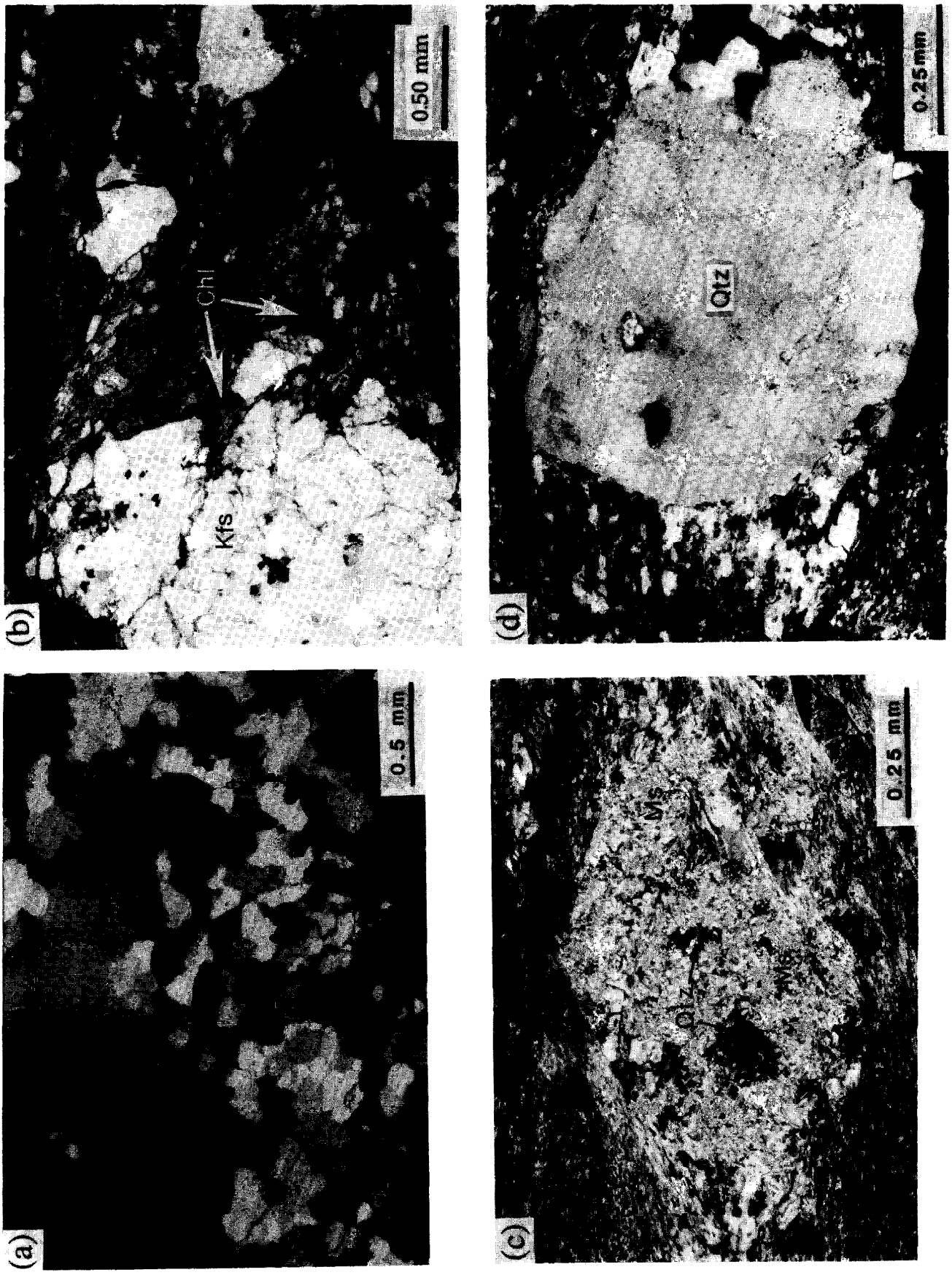

Fig. 5. (a) Plastic deformation features in a quartz porphyroclast of a protomylonite from thermal subzone 2. Recrystallized grains and subgrains are common. Unrecrystallized portions of the porphyroclast show strong undulose extinction. (b) Chlorite fibers growing in the pressure shadow of a K-feldspar porphyroclast in a protomylonite from thermal subzone 2. Chlorite occurs primarily in porphyroclast pressure shadows in these protomylonites along with muscovite and quartz. Minor amounts of chlorite may also be found in the matrix. (c) Augen shaped areas of quartz–muscovite intergrowth in a ultramylonite of thermal subzone 3. These areas represent original K-feldspar or plagioclase porphyroclasts which were altered to muscovite + quartz. Matrix consisting of quartz and muscovite wraps around the augen shaped areas. (d) A relatively undeformed quartz porphyroclast in a ultramylonite from thermal subzone 3. The ultramylonite consists of a few quartz porphyroclasts in a matrix consisting primarily of quartz and muscovite.

feldspar and plagioclase lack any signs of recrystallization and mainly deform by fracturing, indicating temperatures below 500°C. There are many quartz porphyroclasts in these rocks, which show only moderate recrystallization perhaps reflecting lower deformation temperatures than thermal subzone 1 where quartz is extensively recrystallized. Plastic deformation of quartz implies greenschist grade conditions (>350°C); however, even lower temperatures are possible in the presence of fluids (Tullis & Yund 1980, Zadins & Mitra 1986). The presence of biotite suggests temperatures of about 400°C or higher, and provides a lower limit for the temperature of deformation. Secondary epidote found in these rocks probably formed by the following reaction, modified after Bryant (1966) to include Fe-rich epidote and albite (An_{10}) as reactants.

$$\underset{\text{albite } (An_{10})}{2Na_9CaAl_{11}Si_{29}O_{80}} + \underset{\text{K-feldspar}}{4KAlSi_3O_8} + 4K^+ + 3H_2O + 11H^+ + Fe^{3+} = \underset{\text{epidote}}{Ca_2FeAl_2Si_3O_{12}(OH)} + \underset{\text{muscovite}}{8KAl_3Si_3O_{10}(OH)_2} + \underset{\text{quartz}}{43SiO_2} + 18Na^+ \quad (1)$$

Syntectonic chlorite is found throughout the subzone. The association of epidote and chlorite in these granitic mylonites suggests conditions of lowest greenschist grade, as in the case of pelites and graywackes (Winkler 1974). Further, the assemblage muscovite + biotite + quartz + calcite is also characteristic of greenschist grade conditions and probably formed by the following reaction (Drury 1974, Beach 1980).

$$\underset{\text{K-feldspar}}{2KAlSi_3O_8} + \underset{\text{albite } (An_{10})}{Na_9CaAl_{11}Si_{29}O_{80}} + 3(Mg, Fe)^{2+} + 3K^+ + CO_2 + 5H_2O = \underset{\text{muscovite}}{4KAl_3Si_3O_{10}(OH)_2} + \underset{\text{biotite}}{K_2(Mg, Fe)_3AlSi_3O_{10}(OH)_2} + \underset{\text{calcite}}{CaCO_3} + \underset{\text{quartz}}{20SiO_2} + 9Na^+ \quad (2)$$

Evidently, the temperatures of mylonitization in the protomylonites and mylonites of thermal subzone 2 remained within the range of 400–500°C (greenschist grade). The ultramylonites UM-2 and UM-3 consist of very few quartz and feldspar porphyroclasts, and their temperatures of deformation are difficult to assess. These ultramylonites may have formed either at the same time (and thus temperature) as the adjacent mylonites, or during a later reactivation of the mylonite zone (and thus possibly at a lower temperature).

Thermal subzone 3

This subzone consists of ultramylonites (UM-4) which contain more porphyroclasts and a finer matrix than the adjacent mylonites (MY-4) of thermal subzone 2. Porphyroclasts of quartz are most common, K-feldspar porphyroclasts occasionally also occur, but no plagioclase is found probably because of complete sericitization. Potassium-feldspar porphyroclasts (0.15–1.0 mm) show no evidence of plastic deformation and exhibit only minor fracturing, and have been extensively altered to muscovite and quartz. Where K-feldspar is absent, augen shaped areas (1.0–1.5 mm diameter) consisting of fine intergrowths of randomly oriented muscovite and quartz are found, probably representing original feldspar porphyroclasts (Fig. 5c). Deformation of quartz porphyroclasts (2.0–0.50 mm) varies from weak undulose extinction to development of deformation bands and zones of recrystallized grains (0.02–0.05 mm); occasionally an entire porphyroclast is recrystallized. However, in general, the quartz porphyroclasts of this subzone are less deformed (Fig. 5d) than those of the adjacent mylonites (MY-4) of thermal subzone 2. Quartz ribbons consist of recrystallized grains 0.15 mm in diameter. The matrix quartz grains are 0.01–0.05 mm in size. Biotite and muscovite are newly crystallized and occur in distinct separate ribbons. Chlorite is found in one ultramylonite sample within 50 m of the thrust contact. It is intergrown with muscovite and occurs mostly as newly crystallized grains formed during mylonitization, but a small fraction may have formed later by retrogression of biotite.

Temperature of deformation. The temperature of mylonitization for thermal subzone 3 (ultramylonite of UM-4) is more difficult to assess than in the other subzones. Feldspars are rare and are extensively altered, suggesting an abundance of aqueous fluids. As described above, quartz porphyroclasts are more abundant, and relatively less plastically deformed than those in the immediately adjacent mylonites (MY-4) of thermal subzone 2; thus the ultramylonites of UM-4 could not have formed from the mylonites of MY-4. Also, the weaker deformation of quartz cannot be attributed to the absence of aqueous fluids because evidence exists of the presence of fluids in this subzone. We suggest that UM-4 ultramylonites represent a lower temperature deformation than MY-4 mylonites and may have evolved separately from the protolith along a path that included extensive fracturing and alteration of the feldspars resulting in reaction softening (Gilotti 1989) in the zone; the development of a fine grained, weak matrix may partially explain the relatively weak plastic deformation of quartz. Although no specific temperature can be assigned to this deformation, it appears that the temperatures were close to the brittle–plastic transition in quartz (> 350°C). The presence of biotite in the ultramylonites suggests temperatures of at least 400°C. This interpretation is further supported by the deformation observed in the tectonic slices lying immediately

below UM-4 ultramylonites, and the underlying footwall rocks (Srivastava 1992). Deformation at the brittle–plastic transition is observed in the upper tectonic slice where quartz grains show brittle fractures. Progressively lower temperatures of deformation are encountered farther down into the footwall.

DISCUSSION

Conventional geothermobarometric methods are not suitable for obtaining accurate estimates of temperatures of deformation in the NAT zone mylonites for two reasons. Firstly, the chemical processes operating during mylonitization are very complex, and because mylonitization in the case of the NAT zone involved retrogression, it is more difficult to show that assemblages in these mylonites are in equilibrium than in prograde assemblages of metamorphic rocks. Secondly, mineral assemblages found in the NAT zone mylonites are not suitable for using established geothermobarometers. Nevertheless, it is possible to obtain a range of possible mylonitization temperatures from deformation mechanisms of individual minerals and mineral reactions in representative samples from different parts of the NAT zone. It appears that the temperature of deformation decreased continuously from 500–600°C at the top of the mylonite zone to about 400°C near its base. Even lower temperatures of about 350°C were attained in the footwall not far from the thrust. It is assumed that the NAT mylonite zone was uplifted rapidly after its formation, so that the microstructures were frozen in (Knipe 1989), thus reflecting the original range of deformation temperatures.

It follows from the power law equations governing dislocation creep (Elliott 1973, Ashby & Verrall 1978, Schmid 1983) that, for the same grain size and differential stress, an increase in strain rate may have the same effect on deformation mechanisms as a decrease in temperature, and vice versa. For example, a lower temperature deformation seen in feldspars of thermal subzone 2 as compared to the high temperature deformation in feldspars of thermal subzone 1 may also be explained by a higher strain rate in thermal subzone 2. However, the lower temperature deformation in the protomylonites (PM-2) and mylonites (MY-3, MY-4) of the thermal subzone 2 is evident not only from deformation mechanisms but also from mineral assemblages. We have, therefore, assumed that strain rate is approximately constant across the mylonite zone and that temperature is the main factor controlling deformation mechanisms of minerals.

Deformation mechanisms of quartz and feldspar, and various mineral reactions indicate a decrease in the temperature of deformation towards the base of the mylonite zone. Within the mylonite zone, three main zones yielding significantly different temperatures can be identified. The first zone (thermal subzone 1), farthest away from the fault, shows deformation temperatures of 500–600°C. The second zone (thermal subzone 2), closer to the fault, yields deformation temperatures in the range 400–500°C. The third zone (thermal subzone 3), consisting of ultramylonites, indicates deformation temperatures at the brittle–ductile transition for quartz (~400°C). Similar temperatures of deformation are observed in the immediate footwall, and even lower temperatures are encountered farther down into the footwall. The difference in the temperature of deformation between the top and the bottom of the mylonite zone is 100–200°C. Microstructural evidence suggests that each of the three zones evolved separately, each starting with an undeformed protolith and following a slightly different *P–T*–strain path, rather than by continued deformation of rocks similar to those in an adjoining zone.

We attribute the lower temperatures of deformation towards the base of the NAT mylonite zone to a thermal gradient established due to cooling, as suggested by thermal models of *hot* thrust sheets emplaced on cold rocks (Oxburgh & Turcotte 1974, England & Thompson 1984). Active operation of this process in regions of thrust tectonics has been demonstrated by petrologic studies and *P–T–t* path modeling of rocks (Karabinos 1984, Selverstone *et al.* 1984, Chamberlain & Zeitler 1986, Spear *et al.* 1990). Most thermal models (Oxburgh & Turcotte 1974, England & Thompson 1984), however, assume instantaneous thrusting and consider re-equilibration of perturbed isotherms after thrust sheet emplacement, over intervals on the order of 100 Ma. Thermal effects of conductive heat transfer between the hanging wall and footwall rocks *during* thrusting have been modeled by Karabinos & Ketcham (1988). These authors showed that, during thrusting and for geologically relevant parameters, temperatures in the hanging wall may be significantly lowered and those in the footwall raised, over distances of several kilometers from a thrust surface. Because the inverse metamorphic gradient in the NAT mylonite zone is established on the basis of development of deformation textures and mineral reactions accompanying mylonitization, clearly associated with thrusting along the NAT, the heat transfer and associated cooling must have occurred at the time of thrusting. The assumption of conduction as the primary mode of heat transfer (Karabinos & Ketcham 1988) may, however, be unrealistic. There is evidence for abundant fluids in the lower (northern) part of the NAT zone and convective heat transfer by circulating fluids may have played an important role. Convective heat transfer by fluids increases the effective diffusivity of the rocks (Oxburgh & Turcotte 1974), and would serve to enhance the heat transfer during thrusting.

Initially, due to the normal geothermal gradient, the temperatures at the base of the mylonite zone (closest to the thrust) must have been somewhat higher than the temperatures at its top (500–600°C). Therefore, the mylonitic deformation at the base must have started at temperatures in excess of 500–600°C. However, feldspars in the mylonites (MY-3 and MY-4) and ultramylonites (UM-4) near the base of the mylonite zone do not show any evidence of high temperature deformation

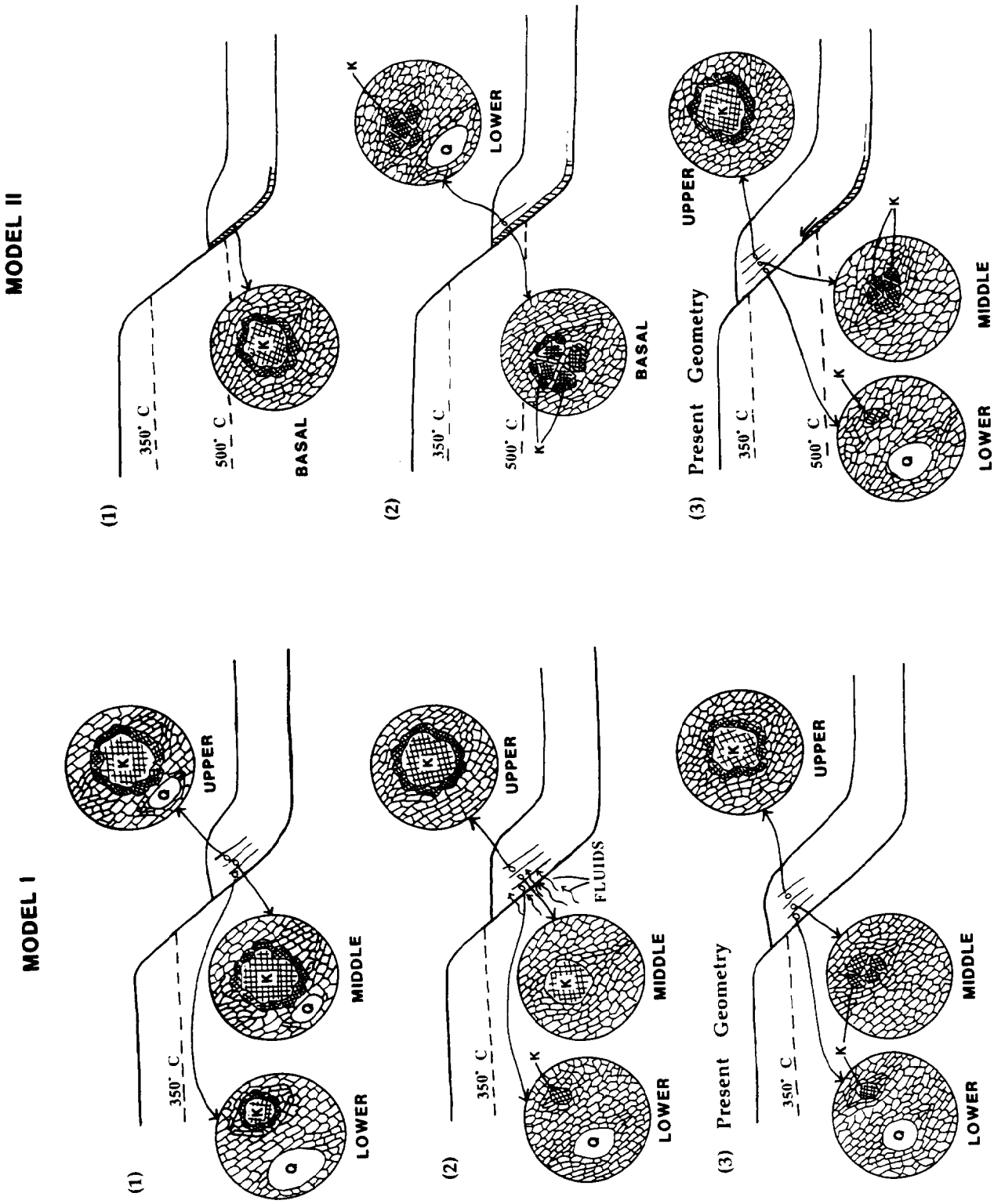

Fig. 6. Two end-member models for the evolution of the NAT mylonite zone in three stages. These models can account for the lack of high temperature deformation microstructures in feldspar near the base of the NAT mylonite zone. In Model I and in Stage 3 of Model II, the thrust zone is schematically shown to consist of three subzones which correspond to the three thermal subzones presently observed. The thickness of these zones and the steepness of the ramp is exaggerated. See text for discussion. Symbols: K—K-feldspar, Q—Quartz. The matrix is schematically shown to consist entirely of recrystallized quartz grains.

(e.g. dynamic recrystallization). We envision two end-member models (Fig. 6) for the formation of the NAT mylonite zone to explain this lack of high temperature deformation near the base of the mylonite zone. According to the first model (Model I, Fig. 6), the initial high temperature deformation due to thrusting may have taken place over a fairly thick zone that included the present mylonite and ultramylonite zones near the base of the mylonite zone. During this deformation, some of the feldspars may have been completely recrystallized while others developed core–mantle structures (Stage 1, Model I, Fig. 6). At this stage, quartz porphyroclasts existed throughout the mylonite zone (Stage 1, Model I, Fig. 6). With further motion along the thrust, the mylonitic rocks were carried to shallower levels, an inverted thermal gradient was set up, and fluids probably entered the mylonite zone from the footwall (Stage 2, Model I, Fig. 6). Recrystallized grains are especially prone to chemical alteration because the larger surface area provides a greater contact with fluids. Recrystallization combined with enhanced alteration probably caused the complete disappearance of feldspars in some cases, while in other cases unrecrystallized cores showing only minor plastic deformation remained (Stage 2, Model I, Fig. 6). This process probably took place selectively near the base of the mylonite zone due to abundance of fluids driven off the footwall. Also, the deformation leading to Stage 2 caused complete recrystallization of quartz porphyroclasts in the upper parts of the mylonite zone, where high temperatures prevailed, but quartz porphyroclasts survived near the base of the mylonite zone, where the temperatures were lower (Stage 2, Model I, Fig. 6). Continued motion along the thrust caused further cooling of the mylonite zone, so that feldspars deformed by fracturing and underwent alteration in the lower part of the mylonite zone, while they continued to deform plastically in the upper part (Stage 3, Model I, Fig. 6).

Alternatively, the initial thrusting related high temperature deformation may have been restricted to a thin zone at the base of the present mylonite zone (Stage 1, Model II, Fig. 6). With continued motion, the hanging wall was brought to shallower levels and cooled, leading to the development of an inverted thermal gradient. Deformation slowly spread upward from the basal mylonite zone and initial deformation in the present mylonite zone, located above the basal zone, probably began at this time (Stage 2, Model II, Fig. 6). The basal mylonite zone which developed at high temperature during the initial stages of deformation probably continued to deform at lower temperatures (Stage 2, Model II, Fig. 6). However, the rocks currently present at the base of the mylonite zone do not show any evidence of overprinting of high temperature deformation by low temperature deformation. It is possible that the basal mylonite zone was left behind as a passive slice because the locus of motion shifted to a higher level (Stage 3, Model II, Fig. 6). The present mylonite zone evolved during motion along this higher thrust, under a pronounced inverted thermal gradient, with lower temperature mylonites and ultramylonites forming close to the thrust and higher temperature mylonites and protomylonites forming farther up into the hanging wall as the deformation spread upward. During this phase of deformation, feldspars underwent fracturing and chemical alteration close to the base of the mylonite zone but deformed by dynamic recrystallization in the upper parts (Stage 3, Model II, Fig. 6).

Both of our models imply that deformation along the fault zone continued and considerable displacement occurred after an inverted thermal gradient had developed along the thrust zone. The actual evolution of the zone may have occurred by a combination of the two models.

CONCLUSIONS

Deformation mechanism and microstructures of mylonites along the North Almora Thrust suggest an inverted thermal profile in the mylonite zone. We interpret the inverted profile to have developed due to syntectonic cooling of the hanging wall *during* thrusting. This study provides evidence that heat transfer may occur effectively by conduction and convection during thrusting and may leave its signatures in the rocks deformed in the process.

Acknowledgements—This research was funded by grants from the Geological Society of America, the Sigma Xi Scientific Society, and the National Geographic Society. We wish to thank Simon Hanmer and Ramon Loosveld for their thorough and helpful reviews of the manuscript. P.S. wishes to thank his numerous field assistants and natives of Kumaon who made field work in the Himalaya a memorable experience. Thanks are also due to Gerry Kloc for preparing excellent thin-sections.

REFERENCES

Aleksandrowski, P. 1985. Graphical determination of principal stress directions for slickenside lineation populations: an attempt to modify Arthaud's method. *J. Struct. Geol.* **7**, 73–82.

Angelier, J. 1979. Determination of the mean principal directions of stresses for a given fault population. *Tectonophysics* **56**, T17–T26.

Arthaud, F. 1969. Méthode de détermination graphique des directions de reccourcisement, d'allongment et intermédiaire d'une population de failes. *Bull. Soc. Geol. Fr.* **7**(11), 729–737.

Ashby, M. F. & Verrall, R. A. 1978. Micromechanisms of flow and fracture and their relevance to the rheology of the upper mantle. *Phil. Trans. R. Soc. Lond.* **A288**, 59–95.

Beach, A. 1980. Retrogressive metamorphic processes in shear zones with special reference to the Lewisian complex. *J. Struct. Geol.* **2**, 257–263.

Bell, T. H. & Johnson, S. E. 1989. The role of deformation partitioning in the deformation and recrystallization of plagioclase and K-feldspar in the Woodroffe thrust mylonite zone, central Australia. *J. Metamorph. Geol.* **7**, 151–168.

Brown, W. L., Macaudiere, J., Ohnenstetter, D. & Ohnenstetter, M. 1980. Ductile shear zones in a meta-anorthosite from Harris, Scotland: textural and compositional changes in plagioclase. *J. Struct. Geol.* **2**, 281–287.

Bryant, B. 1966. Formation of phyllonites in the Grandfather mountain area, northwestern North Carolina. *Prof. Pap. U.S. Geol. Surv.* **550-D**, 144–150.

Chamberlain, C. P. & Zeitler, P. 1986. Pressure–temperature–time paths in the Nanga Parbat massif: constraints on the tectonic

development of the northwest Himalaya. Abstract, *Prog. geol. Soc. Am.* **18**, 561.

Debat, P., Soula, J.-C., Kubin, L. & Vidal, J.-L. 1978. Optical studies of natural deformation microstructures in feldspars (gneiss and pegmatites from Occitania Southern France). *Lithos* **11**, 133–145.

Drury, S. A. 1974. Chemical changes during retrogressive metamorphism of Lewisian granulite facies rocks from Coll and Tiree. *Scott. J. Geol.* **10**(3), 237–256.

Elliott, D. 1973. Diffusion flow laws in metamorphic rocks. *Geol. Soc. Am. Bull.* **84**, 2645–2664.

England, P. E. & Thompson, A. B. 1984. Pressure–temperature–time paths of regional metamorphism I. Heat transfer during the evolution of regions of thickened continental crust. *J. Petrol.* **25**, 894–928.

Etheridge, M. A. & Hobbs, B. E. 1974. Chemical and deformational controls on recrystallization of mica. *Contra. Miner. Petrol.* **43**, 111–124.

Ghose, A., Chakrabarti, B. & Singh, R. K., 1974. Structural and Metamorphic history of the Almora Group, Kumaon Himalaya, U.P. *Himalayan Geol.* **4**, 171–194.

Gilotti, J. A. 1989. Reaction progress during mylonitization of basaltic dikes along the Särv thrust, Swedish Caledonides. *Contr. Miner. Petrol.* **101**, 30–45.

Hanmer, S. K. 1982. Microstructure and geochemistry of plagioclase and microcline in naturally deformed granite. *J. Struct. Geol.* **4**, 197–213.

Hobbs, B. E., Means, W. D. & Williams, P. F. 1976. *An Outline of Structural Geology*. Wiley, Singapore.

Karabinos, P. 1984. Deformation and metamorphism on the east side of the Green Mountain massif in southern Vermont. *Bull. geol. Soc. Am.* **95**, 584–593.

Karabinos, P. & Ketcham, R. 1988. Thermal structure of active thrust belts. *J. Metamorph. Geol.* **6**, 559–570.

Kerrich, R. & Hyndman, D. W. 1986. Thermal and fluid regimes in the Bitterroot lobe–Sapphire block detachment zone, Montana: evidence from $^{18}O/^{16}O$ and geological relations. *Geol. Soc. Am. Bull.* **97**, 147–155.

Kerrich, R., La Tour, T. E. & Willmore, L. 1984. Fluid participation in deep fault zones: Evidence from geological, geochemical, and $^{18}O/^{16}O$ relations. *J. geophys. Res.* **89**, 4331–4343.

Knipe, R. J. 1989. Deformation mechanisms—recognition from natural tectonites. *J. Struct. Geol.* **11**. 127–146.

Kretz, R. 1983. Symbols for rock forming minerals. *Am. Miner.* **68**, 277–279.

La Tour, T. & Barnett, R. L. 1987. Mineralogical changes accompanying mylonitization in the Bitterroot dome of Idaho batholith: implications for timing of deformation. *Geol. Soc. Am. Bull.* **98**, 556–563.

Marshak, S. & Mitra, G. 1988. *Basic Methods of Structural Geology*. Prentice Hall, Englewood Cliffs, New Jersey.

Mitra, G. 1978. Ductile deformation zones and mylonites: the mechanical processes involved in the deformation of crystalline basement rocks. *Am. J. Sci.* **278**, 1057–1084.

Molnar, P. & Tapponnier, P. 1975. Cenozoic tectonics of Asia: effects of a continental collision. *Science* **189**, 419–426.

Oxburgh, E. R. & Turcotte, D. L. 1974. Thermal gradients and regional metamorphism in overthrust terrains with special reference to the Eastern Alps. *Schweiz. miner. petrogr. Mitt.* **54**, 641–662.

Powell, C. McA. 1979. A speculative tectonic history of Pakistan and surroundings: some constraints from the Indian Ocean. In: *Geodynamics of Pakistan* (edited by Farah, A. and DeJong, K. A.). *Geol. Surv. Pakistan*, Quetta, Pakistan, 5–24.

Schmid, S. M. 1983. Microfabric studies as indicators of deformation mechanisms and flow laws operative in mountain building. In: *Mountain Building Processes* (edited by Hsu, K. J.). Academic Press, 95–110.

Searle, M. P., Windley, B. F., Coward, M. P., Cooper, D. J. W., Rex, A. J., Rex, D., Tingdong, L., Xuchang, X., Jan, M. Q., Thakur, V. C. & Kumar, S. 1987. The closing of the Tethys and the tectonics of the Himalaya. *Geol. Soc. Am. Bull.* **98**, 678–701.

Selverstone, J., Spear, F. S., Franz, G. & Morteani, G. 1984. High-pressure metamorphism in the SW Tauern Window, Austria: *P–T* paths from hornblende–kyanite–staurolite schists. *J. Petrol.* **25**, 501–531.

Simpson, C. 1985. Deformation of granitic rocks across the brittle–ductile transition. *J. Struct. Geol.* **7**, 503–511.

Spear, F. S., Hickmott, D. D. & Selverstone, J. 1990. Metamorphic consequences of thrust emplacement, Fall Mountain, New Hampshire. *Geol. Soc. Am. Bull.* **102**, 1344–1360.

Srivastava, P. 1992. Stratigraphy, deep structure, and structural evolution of the Kumaon and Garhwal Himalaya (India). Unpublished Ph.D. thesis, University of Rochester, New York.

Srivastava, P. & Mitra, G. 1994. Thrust geometries and deep structure of the outer and lesser Himalaya, Kumaon and Garhwal (India): implications for evolution of the Himalayan fold-and-thrust belt. *Tectonics* **13**, 89–109.

Trivedi, J. R., Gopalan, K. & Valdiya, K. S. 1984. Rb–Sr ages of granitic rocks within the Lesser Himalayan nappes, Kumaon. *J. geol. Soc. India* **25**, 641–654.

Tullis, J. 1983. Deformation of feldspars. In: *Feldspar Mineralogy* (edited by Ribbe, P.H.). *Miner. Soc. Am.*, Washington, DC, 297–323.

Tullis, J. and Yund, R. A. 1980. Hydrolytic weakening of experimentally deformed Westerly granite and Hale albite rock. *J. Struct. Geol.* **2**, 439–451.

Tullis, J. & Yund, R. A. 1985. Dynamic recrystallization of feldspar: a mechanism for ductile shear zone formation. *Geology* **13**, 238–241.

Valdiya, K. S. 1980. *Geology of Kumaon Lesser Himalaya*. Wadia Institute of Himalayan Geology, Dehradun, India.

Vernon, R. H. 1975. Deformation and recrystallization of a plagioclase grain. *Am. Miner.* **60**, 884–888.

Vidal, J.-L., Kubin, L., Debat, P. & Soula, J.-C. 1980. Deformation and dynamic recrystallization of K-feldspar augen in orthogneiss from Montagne Noire, Occitania, Southern France. *Lithos* **13**, 247–255.

Voll, G. 1976. Recrystallization of quartz, biotite, and feldspars from Erstfeld to the Leventina Nappe, Swiss Alps and its geological significance. *Schweiz. miner. petrogr. Mitt.* **56**, 641–647.

White, S. 1975. Tectonic deformation and recrystallization of oligoclase. *Contr. Miner. Petrol.* **50**, 287–304.

White, S. 1976. The effects of strain on microstructures, fabric and deformation mechanisms in quartzites. *Phil. Trans. R. Soc. Lond.* **A283**, 69–86.

Wilson, P. F. & Bell, I. A. 1979. Deformation of biotite and muscovite: optical microstructures. *Tectonophysics* **58**, 179–200.

Winkler, H. G. F. 1974. *Petrogenesis of Metamorphic Rocks*. Springer, New York.

Zadins, Z. Z. & Mitra, G. 1986. Brittle–ductile deformation along thrust faults, an example from the Hudson Valley thrust belt. *Geol. Soc. Am. Ann. Mtg Abs.* **18**, 799.